Intercomparison of Inversion Algorithms to Retrieve Rain Rate From SSM/I by Using an Extended Validation Set Over the Mediterranean Area

Nazzareno Pierdicca, *Member, IEEE*, Luca Pulvirenti, Frank Silvio Marzano, *Senior Member, IEEE*, Piero Ciotti, *Member, IEEE*, Patrizia Basili, *Member, IEEE*, and Giovanni d'Auria

***Abstract*—The capability of some inversion algorithms to estimate surface rain rate at the midlatitude basin scale from the Special Sensor Microwave Imager (SSM/I) data is analyzed. For this purpose, an extended database has been derived from coincident SSM/I images and half-hourly rain rate data obtained from a rain gauge network, placed along the Tiber River basin in Central Italy, during nine years (from 1992 to 2000). The database has been divided in a training set, to calibrate the empirical algorithms, and in a validation one, to compare the results of the considered techniques. The proposed retrieval methods are based on both empirical and physical approaches. Among the empirical methods, a regression, an artificial feedforward neural network, and a Bayesian maximum *a posteriori* (MAP) inversion have been considered. Three algorithms available in the literature are also included as benchmarks. As physical algorithms, the MAP method and the minimum mean square estimator have been used. Moreover, in order to test the behavior of the algorithms with different kinds of precipitation, a classification of rainy events, based on some statistical parameters derived from rain gauge measurements, has been performed. From this classification, an attempt to identify the type of event from radiometric data has been carried out. The purposes of this paper are to determine whether the use of an extended training set, referred to a limited geographical area, can improve the SSM/I skill in rain detection and estimation and, mainly, to confirm the validity of the physical approach adopted in previous works. It will be shown that, among all the estimators, the neural network presents the best performances and that the physical techniques provide results only slightly worse than those given by empirical methods, but with the well-known advantage of an easy application to different geographical zones and different sensors.**

***Index Terms*—Atmospheric remote sensing, clouds and precipitation, microwave radiative transfer, spaceborne microwave radiometry.**

I. Introduction

SPACEBORNE microwave radiometry represents a key technique for remotely sensing atmospheric precipitation [1], [2]. The relatively low cost of a wide-swath scanning instrument (with respect to radar technology) and its fairly high sensitivity to the hydrometeor vertical structure (with respect to visible/infrared radiometers) are the outstanding features of this methodology. However, major drawbacks are still present in its use, especially referring to the quite low spatial resolution [3] (not less than a few kilometers so far for spaceborne sensors) and to its difficulty to detect and estimate rainfall over land, particularly in the case of rain produced by stratiform clouds [4]. Such poor sensitivity over land is mainly due to the small contrast between rainfall radiometric and surface signatures and also to the variability of land surface emissivity within the low-resolution pixels. On the other hand, rainfall over land is one of the foremost goals of spaceborne monitoring because of its relevant impact on human social activities.

In order to retrieve surface rain rate from microwave radiometric data, two different approaches can be followed: physical or empirical ones. The former is based on dynamical cloud-resolving models able to simulate the precipitation microphysics and on radiative transfer models to associate to each cloud structure a vector of simulated brightness temperatures [1], [5]–[7]. This approach permits to properly take into account thermodynamic, geometrical, and dielectric parameters that characterize an absorbing and scattering atmosphere [8]. For the purpose of reducing the dependence of the retrieval capability on the season and on the climatology of the geographical area of interest, local parameters and their seasonal variability, such as the vertical profiles of humidity and temperature, the cloud top and base heights, and clear-air land emissivities, can be introduced, as constraints, in the simulation process [9]. Physical methods give appreciable results only if these local parameters are estimated with sufficient accuracy.

The empirical approach is based on coincident and colocated spaceborne and ground data [10]–[12]. Two major sources of rainfall ground data may be available. The first is represented by weather Doppler radars at S- or C-band, in which the scans at the lowest elevation angle are used to statistically convert measured rain reflectivity to rain rate. Areas of several hundreds of kilometers can be covered and mapped with a horizontal resolution of a few kilometers. Although several works have shown that the quality of radar rain rate data was often questionable, thus suggesting a careful calibration of radar-derived maps by rain gauges observations [13], [14], in the last decade, there has been a major effort to improve the consistency of radar data. However, river basins cannot be covered by a single radar, and natural obstacles (such as hills and mountains) can cause

Manuscript received September 30, 2003; revised April 2, 2004. This work was supported by the Italian Space Agency (ASI).

N. Pierdicca, L. Pulvirenti, and G. d'Auria are with the Department of Electronic Engineering, University of Rome "La Sapienza," 00184 Roma, Italy (e-mail: nazzareno.pierdicca@uniroma1.it; pulvirenti@mail.die.uniroma1.it; dauria@mail.die.uniroma1.it).

F. S. Marzano and P. Ciotti are with the Department of Electrical Engineering, Center of Excellence CETEMPS, University of L'Aquila, 67040 L'Aquila, Italy (e-mail: marzano@ing.univaq.it;).

P. Basili is with the Department of of Electronic and Information Engineering, University of Perugia, 06125 Perugia, Italy (e-mail: basili@diei.unipg.it).

Digital Object Identifier 10.1109/TGRS.2004.834651

a high percentage of radar beam blockage, thus impeding direct near-surface rain retrievals. The second source of rain data is represented by rain gauge networks. They inherently provide surface rain measurements and, especially at a basin scale, can represent a valuable monitoring tool, in most cases associated to hydrological data about river flow and runoff. The network spatial density is a crucial aspect, which can raise a sampling error difficult to quantify. Moreover, tipping-bucket measurements can be affected by uncertainties due to wind shear and iced hydrometeors.

Empirical techniques are generally simple to be implemented, while especially over land, cloud and surface radiative modeling is very complicated. On the other hand, physical techniques can be easily extended to regions different from the training one and to new sensors having different channels, resolutions, and/or scanning geometry.

In previous papers, we focused our interest on physical approaches [6], [9], [15]. In this paper, empirical algorithms are also taken into consideration, and a comparison between the performances of the different techniques is presented. This paper investigates the improvement of the capability of a spaceborne radiometer to detect and estimate precipitation achieved through the use of an extended database, referred to a limited geographical area. Moreover, it aims to confirm the validity of the physical approach adopted in previous works by showing that it gives results quite similar to those provided by empirical methods calibrated over the area of interest. In this context, a new inversion scheme based on the minimum mean square estimator (MMSE) is introduced. With respect to other works concerning the intercomparison of SSM/I retrieval methods, we would like to point out the importance of considering a nine-year dataset, an aspect which makes the validation very reliable for our geographical area of interest.

As a source of spaceborne radiometric data, the Special Sensor Microwave/Imager (SSM/I) has been used. Precipitation measurements have been obtained from a rain gauge network placed along the Tiber River basin in Central Italy. In Section II, a short overview of the two instruments is given and the generation of a combined database of brightness temperatures and surface rain rates is depicted. Detection of rainy events is generally needed by physical retrievals before applying the inversion methods. Moreover, discrimination of the events in different categories (i.e., stratiform and convective) may also make more accurate the training phase of the empirical algorithms. For this reason, the problem of the detection of rainy events and their classification either from rain gauge data or from radiometric measurements is considered in Section III. In Section IV, the three empirical techniques considered in this paper are introduced. The first one is a linear regression, the second one is based on an artificial feedforward neural network, and the third one is the Bayesian maximum *a posteriori* (MAP) probability criterion. Three algorithms available in literature are also included and used as benchmarks in the comparison. In Section V, the physical approach is summarized. In previous works, only the MAP inversion scheme has been considered, while as mentioned above, in this paper, the MMSE is used as well. The mathematical details of both Bayesian techniques are given in the Appendix. In Section VI, a comparison of the results provided by the different algorithms is illustrated, in terms of their capability to reproduce the precipitation measured on ground. The entire database of brightness temperatures and rain rate measurements has been divided into training and validation sets to perform an independent test of the retrieval accuracies of empirical methods. Even though a brief mention concerning the results at pixel level is provided, the comparison has been carried out at basin level (i.e., by computing the mean value of rain rate in the basin) to overcome the radiometric pixel geolocation errors and the different spatial resolution of the two considered instruments, which make the comparison between single pixel measurements very cumbersome, especially if the complex relief of the area of interest is considered. The performances have been also evaluated by considering separately the events classified as stratiform and convective in the validation set.

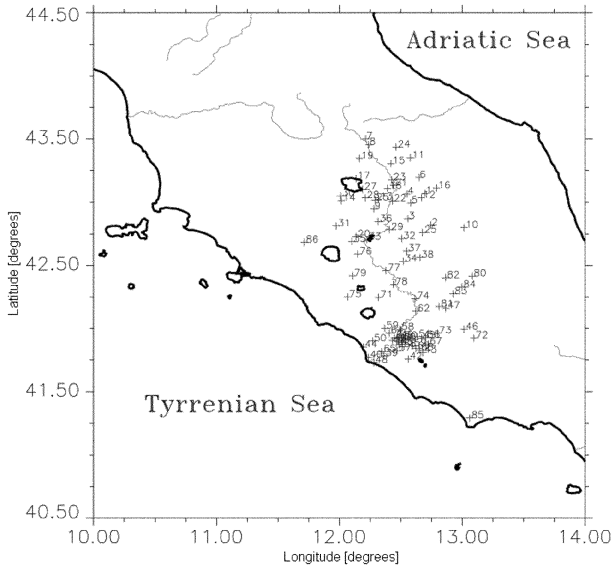

Fig. 1. Rain gauge network of the Tiber River basin. The location of each station is indicated by a cross and the index ranges from 1 to 86 (the maximum number of active rain gauges).

II. Rain Gauge and Satellite Data

As mentioned, the surface precipitation data are represented by the measurements of a rain gauge network located along the Tiber River valley in Central Italy. Stratiform rainy events are very common over a midlatitude geographical zone, while the considered basin is also characterized by convective events occurring when the mean air temperature and the moisture content are both relatively high (conditions leading, when dynamical factors are favorable, to severe precipitation). The local orography is quite complex, and the surface background cannot be considered radiometrically homogeneous. Fig. 1 shows the location of the rain gauges: the network covers a geographical area of about 17 000 km^2. Available data from tipping-bucket rain gauges contain the cumulative precipitation, sampled twice per hour with a resolution of 0.2 mm. The cumulative precipitation has been converted into rain intensity in millimeters per hour. We have collected precipitation data throughout a period of nine years (from 1992 to 2000) for the purpose of building

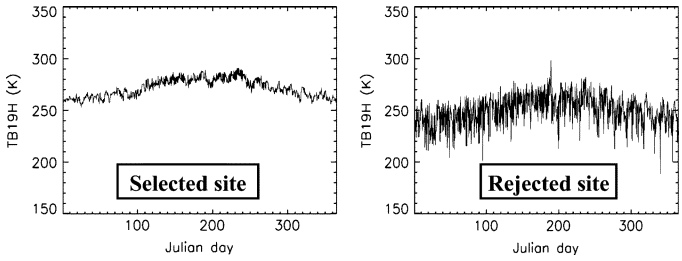

Fig. 2. Comparison between the annual trends of the 19-GHz brightness temperature in horizontal polarization of (a) a rain gauge whose data have been used in the analysis and of (b) a rejected one.

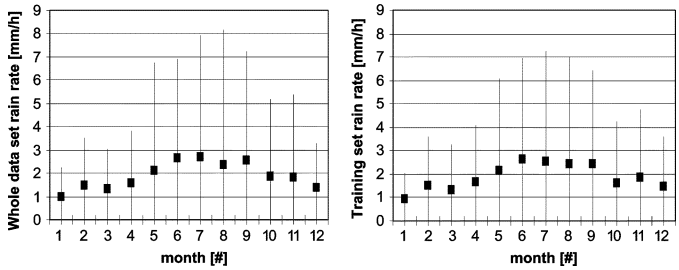

Fig. 3. Annual variation of rain rate for both (a) the whole database and (b) for the training subset. Mean values as well as the ± 1 standard deviation are reported.

reliable training and test sets in terms of precipitation types and seasonal conditions. Even though errors may also affect tipping-bucket measurements, we believe that their good resolution, and sufficiently high spatial density in the area of interest, together with the consideration of such a long period of time, makes our precipitation data reliable enough to be considered as a "ground-truth." The number of active rain gauge stations in the considered period ranges from a minimum of 46 in 1992 to a maximum of 86 in 1995. The network is remotely monitored in near real time, and some lack of data can occasionally occur because of interruptions in the communication link. Notice that, unfortunately, the basin is not covered by weather radar monitoring.

The spaceborne microwave radiometric data have been derived from the SSM/I. This radiometer is installed on board the Defense Meteorological Satellite Program (DMSP) platforms which fly on a near-polar sun-synchronous orbit at an altitude of about 830 km. SSM/I is a multifrequency microwave radiometer that measures brightness temperature (T_{B}) at four frequency bands (i.e., 19.35, 22.2, 37.0, and 85.5 GHz) and at two linear polarizations (i.e., horizontal and vertical), apart from the 22.2-GHz channel which only operates in the vertical polarization. During each conical scan, SSM/I gathers data at an off-nadir observation angle of 53.1° with a swath width of about 1400 km. The spatial resolution is 69×43, 60×40, 37×29, and 15×13 km^2 for the 19-, 22-, 37-, and 85-GHz channels, respectively [16]. The radiometric resolution is better then 0.9 K in each channel. The data geolocation error can theoretically be better then ± 10 km by using the satellite effemerides and a post-processing algorithm.

The coupling of SSM/I measurements and rain gauge data requires, as a first step, to create a database referring to the same (or nearest) acquisition time and geographical location. For each rain gauge site, the closest SSM/I measurement both in time and space has been identified for the low- and the high-resolution channels. Considering the time sampling of the rain gauges, a temporal error of ± 15 min within the combined database may exist. The spatial error is related to the accuracy of SSM/I pixel geolocation which may be often lower then the nominal one (10 km). The maximum accepted distance between rain gauge location and 85-GHz pixel center has been assumed equal to 7 km. A preliminary quality control has been performed to reject the rain gauge sites where the corresponding T_{B} values were affected by the presence of the coastline. For this purpose, SSM/I pixels labeled as coast have been disregarded, while those close to them have been included in the analysis only if their clear-air temporal trend at 19 GHz was within an expected range of variability. In fact, the low emissivity of the sea surface causes sharp depression in the temporal trend of contaminated brightness temperatures as illustrated in Fig. 2, in which a comparison between the annual trends characteristics of a selected site and a rejected one is presented.

Finally, the resulting database consists of 6239 SSM/I passes with about 30% of these related to rainy events (i.e., at least one rain gauge detected rain). The features of this database are resumed in Table I. For the purpose of training the empirical algorithms and testing the different behaviors of all the considered techniques, the database has been divided into training and validation sets by using a systematic sampling. We have temporarily ordered the database and, following this order, we have associated the first SSM/I overpass to the training set, the successive to the test one, etc.. In other words, the 6239 overpasses have been identified by an index, and those having an odd index have been included in the training set, while the even ones in the validation set. The training set is able to reproduce the statistical features of the rainy events belonging to the whole database as it can be observed in Fig. 3, which reports the annual variation of mean event magnitude (in terms of monthly mean value plus and minus standard deviation) for both the mentioned sets of data. From Fig. 3, it emerges that rainy events occurring during summer in the area of interest are fairly intense, although they are more frequent in the other seasons.

III. Classification of Rainy Events

In this section, we describe a procedure which has led us to define two categories of rainy events according to the "ground truth" furnished by the rain gauge network. The first, characterized by moderate and uniform precipitations, has been identified as stratiform and the second, presenting opposite features, as convective. Obviously, a third class had to be added, representing the absence of precipitation. Such classification, based on some statistical parameters derived from our half-hourly rain gauge measurements, aims both to test the behavior of the considered retrieval techniques for different types of precipitation and to assess the capability of a spaceborne microwave radiometer to detect rain, which can be considered as a first step for retrieving rain rate from radiometric data, in particular when physical techniques are adopted.

TABLE I
CHARACTERISTICS OF THE NINE-YEAR DATASET. FOR EACH YEAR, THE NUMBER OF ACTIVE RAIN GAUGES OF THE SSM/I OVERPASSES OVER CENTRAL ITALY AND OF THE OVERPASSES CORRESPONDING TO AT LEAST ONE RAIN GAUGE DETECTING RAIN ARE INDICATED. DMSP F13 AND F14 PLATFORMS HAVE BEEN CONSIDERED

year	N° rain gauges	N° SSM/I passes	N° SSM/I passes with rain rate > 0
1992	47	228	68 (29.8 %)
1993	78	400	77 (19.2 %)
1994	78	229	52 (22.7 %)
1995	86	634	192 (30.3 %)
1996	85	960	365 (38.0 %)
1997	85	515	138 (26.8 %)
1998	85	1093	272 (24.9 %)
1999	85	1085	328 (30.2 %)
2000	83	1095	379 (34.6 %)
total	-	6239	1871 (30.0 %)

The availability of information about the type of precipitation has permitted us to train the empirical methods, which will be described in Section IV, in different ways, incorporating or not the *a priori* information about both the presence and the type of a rainy event and to investigate how this information influences the retrieval accuracy.

A. Classification Based on Rain Gauge Data

Provided the availability of rain gauge data every 30 min in the Tiber River basin, we have considered, as rainy, an event formed by a set of consecutive temporal samples (1 sample = 1/2 h) in which at least one rain gauge detects rain. In this section, M indicates the number of temporal samples of the event, N the number of active rain gauges, i and j represent the rain gauge index and the temporal sample index, respectively, and R indicates rain rate intensity. All the events whose length exceeded 6 h have been divided in subevents in order to avoid including inhomogeneous rainy regimes in the same event.

The following two parameters have been defined to represent the intensity of the event. They are the medium rain rate $(\langle R \rangle)$ and the maximum rain rate $(R_{\max})$, expressed as follows:

$$\langle R \rangle = \frac{1}{M} \sum_{j=1}^{M} \frac{1}{N} \sum_{i=1}^{N} R_{ij} \tag{1}$$

$$R_{\max} = \max(R_{ij}). \tag{2}$$

The next two parameters have been defined to provide an indication about the uniformity of the events from both the temporal and the spatial point of view. They are the spatial standard deviation averaged in time and the temporal standard deviation averaged in space. The former is given by

$$\langle ds \rangle_t = \frac{1}{M} \sum_{j=1}^{M} \left[\frac{1}{N-1} \sum_{i=1}^{N} (R_{ij} - \overline{R_j})^2 \right]^{1/2}. \tag{3}$$

The latter is expressed by

$$\langle dt \rangle_s = \frac{1}{N} \sum_{i=1}^{N} \left[\frac{1}{M-1} \sum_{j=1}^{M} (R_{ij} - \overline{R_i})^2 \right]^{1/2}. \tag{4}$$

As mentioned, all these parameters have been used to split our database into two classes. For this purpose an unsupervised Isodata algorithm [17] has been applied by imposing two output classes. Isodata classification begins by evenly distributing class means in a multidimensional space (in ourcase, the dimension is 4, i.e., the number of parameters defined above). Then, it iteratively clusters the remaining pixels according to the minimum distance from the cluster centers. Each iteration recalculates means and reclassifies pixels with respect to the new means. This process continues until the number of pixels in each class changes by less than a fixed threshold or the maximum number of iterations is reached. Following the Isodata application we have identified 87% of rainy events as stratiform and 13% as convective. The events characterized by high values of $\langle ds \rangle_{\rm t}$ and $\langle dt \rangle_{\rm s}$ have been generally classified as convective. Fig. 4 shows the scatterplot of $\langle dt \rangle_{\rm s}$ versus $\langle ds \rangle_{\rm t}$. The correlation coefficient is 0.79.

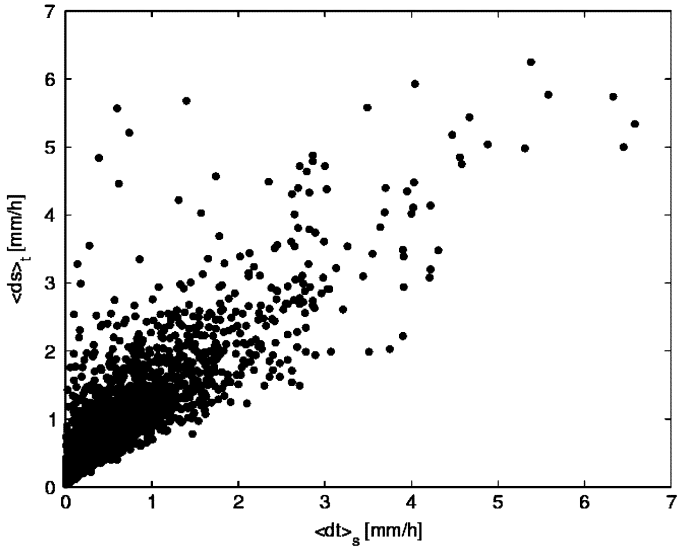

Fig. 4. Scatterplot of the temporal standard deviation averaged in space $\langle dt \rangle_{\rm s}$ versus the spatial standard deviation averaged in time $\langle ds \rangle_{\rm t}$.

B. Rain Detection and Event Classification Based on Satellite Data

The detection of rain from spaceborne microwave Thanradiometric measurements over land is mainly determined by the depression of the 85-GHz $T_{\rm B}$ caused by the scattering produced by the frozen hydrometeors [4], [12]. This means that only convective cloud systems, with precipitating ice, can be easily revealed, while if a cloud is formed mainly by liquid particles, as in the case of a stratiform one, the sensor does not always detect it, and the algorithms may fail to retrieve rainfall.

TABLE II
CONFUSION MATRIX SHOWING THE RESULTS OF THE CLASSIFICATION OF THE EVENTS IN NONRAINY, STRATIFORM, AND CONVECTIVE PERFORMED BY USING SSM/I DATA. THE CLASSIFICATION BASED ON RAIN GAUGE DATA IS CONSIDERED AS THE TRUTH, AND THE SUM OF THE ELEMENTS OF EVERY ROW IS EQUAL TO 1

	Non-rainy events (radiometric data)	**Stratiform events** (radiometric data)	**Convective events** (radiometric data)
Non-rainy events (rain gauge data)	0.65	0.20	0.15
Stratiform events (rain gauge data)	0.31	0.46	0.23
Convective events (rain gauge data)	0.07	0.09	0.84

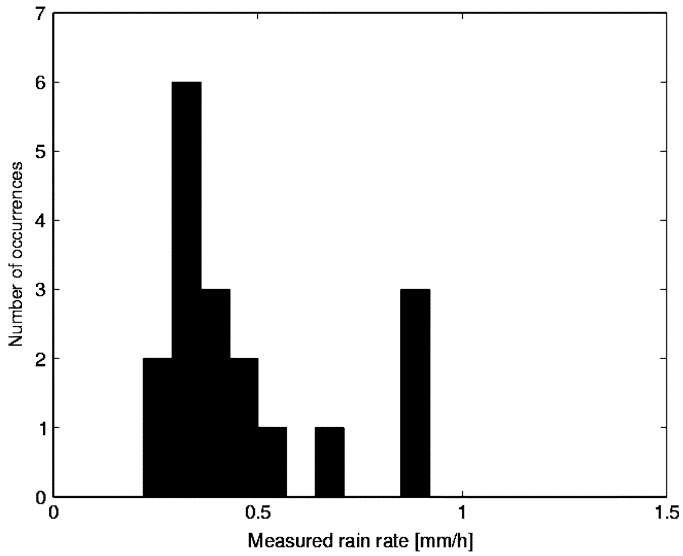

Fig. 5. Histogram of the rain rate measured by the rain gauge network and averaged over the basin for the stratiform events erroneously identified as nonrainy. Only rain rates equal at least to 0.2 mm/h are considered.

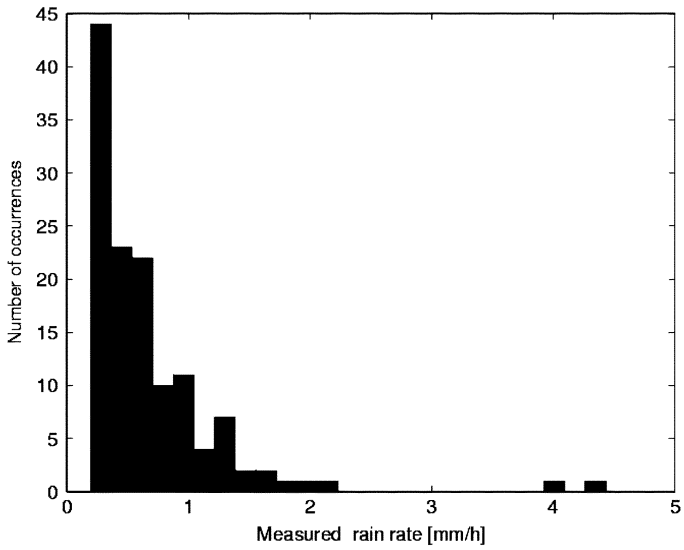

Fig. 6. Histogram of the rain rate measured by the rain gauge network and averaged over the basin for the stratiform events correctly classified. Only rain rates equal at least to 0.2 mm/h are considered.

However, some attempts can be found in literature to identify stratiform precipitation from radiometric data [18], [19].

Here, we investigate about the possibility to discriminate among nonrainy, stratiform, and convective events from SSM/I measurements by using, as reference information, the classification performed by the Isodata algorithm based on the rain gauge data. The discrimination problem basically coincides with that described in part A of the Appendix, where the empirical MAP is concerned. In this case, the class k ($k = 1$ nonrainy, $k = 2$ stratiform, $k = 3$ convective) takes the place of the rain bin $R(i)$. Without going into details, a simplified version is introduced here. If we indicate with $\mathbf{t}_{\mathrm{m}}$ the seven-component vector of multifrequency and multipolarization T_{B} measurements, the mean T_{B} vectors $\langle \mathbf{t}_m^h(k) \rangle$ and the covariance matrices $\mathbf{C}_k^h$ within each class k have been computed for each month h (h ranging from 1 to 12). For each pixel of a SSM/I image belonging to the test set, we have found the class k that minimizes the following distance:

$$d^h(k) = \left[\mathbf{t}_m - \left\langle \mathbf{t}_m^h(k) \right\rangle\right]^T \left[\mathbf{C}_k^h\right]^{-1} \left[\mathbf{t}_m - \left\langle \mathbf{t}_m^h(k) \right\rangle\right], \quad k = 1, \ldots, 3. \quad (5)$$

Finally, we have associated the SSM/I image to a nonrainy, stratiform, or convective event if most of the pixels colocated with rain gauges were classified into class k equal to 1, 2, or 3, respectively.

We have assessed the accuracy of the procedure on the test set by comparing $\mathbf{t}_{\mathrm{m}}$ classification with that furnished by the Isodata algorithm. The results, in terms of confusion matrix, are reported in Table II. The classification based on rain gauge data has been considered as the truth, and the sum of the elements of every row is equal to 1. The good capability to detect convective rain can be noticed, with 84% of correct classification. The major difficulty consists of identifying stratiform events, with 46% of correct classification. This could be expected, since it is well known that shallow clouds have an ambiguous signature with respect to the land background. Thirty-one percent of stratiform events classified as nonrainy can represent a problem, since it may lead to missed detection of possible intense precipitation. To analyze this aspect we have produced the histogram of measured rain rate averaged over the basin for the stratiform events erroneously identified as nonrainy. This is shown in Fig. 5 where only mean rain rates greater than 0.2 mm/h have been included for the sake of plot clarity. Even though 31% of missed detection could seem a quite poor result, it can be observed that the mean precipitation of undetected stratiform events is never more than 0.9 mm/h and that the number of occurrences is low. Therefore, the most part of the errors is made for situations characterized by very low rain values (rain rate averaged over the basin less than 0.2 mm/h). Fig. 6 shows the same histogram for the stratiform events correctly classified. The number of occurrences of

events with detectable precipitation is higher, and the situations in which the mean rain rate reaches values approximately equal to 4 mm/h are revealed.

It is important to notice that the purpose of this procedure is to carry out a preliminary screening of the rainy event from SSM/I data in order to select the proper retrieval algorithm according to the event characteristics, as will be explained in Section VI. Furthermore, the classification is defined having as a reference the rain-gauge-based discrimination, which is in its way arbitrary and must be taken with caution.

IV. Empirical Inversion Techniques

The considered techniques are described in this section, together with a brief sketch of three other methods published in literature.

As in the previous section, the multifrequency T_{B} vector will be indicated by $\mathbf{t}_{\mathrm{m}}$, and rain rate in millimeters per hour will be represented by R. Uppercase bold letters will denote matrices.

A. Regression

If a linearized relationship is assumed between the vector of predictors $\mathbf{p}_{\mathrm{m}}$ and the parameter to be estimated, then the regressive estimation of R is given by

$$\hat{R}_{\mathrm{REG}} = b + \mathbf{D}\mathbf{p}_{\mathrm{m}} = b + \mathbf{C}_{\mathrm{Rp}}\mathbf{C}_{\mathrm{p}}^{-1}\mathbf{p}_{\mathrm{m}} \tag{6}$$

where $\mathbf{D}$ is the regression coefficient matrix, which minimizes the mean square error (MSE) of the estimates with respect to the true values of R, b is the bias, and $\mathbf{C}_{\mathrm{Rp}}$ and $\mathbf{C}_{\mathrm{p}}$ are the cross-covariance matrix between R and $\mathbf{p}_{\mathrm{m}}$ and the autocovariance matrix of $\mathbf{p}_{\mathrm{m}}$, respectively. In (6), we have used $\mathbf{p}_{\mathrm{m}}$ instead of $\mathbf{t}_{\mathrm{m}}$ because, in order to account for nonlinearity in the relationship between satellite observations and surface precipitation, the vector of predictors can generally contain powers of $\mathbf{t}_{\mathrm{m}}$ components. In particular, we have adopted a polynomial expansion to second order so that (6) assumes the following form:

$$\hat{R}_{\mathrm{REG}} = a_0 + \sum_{k=1}^{7}\left(a_{1k}T_{Bk} + a_{2k}T_{Bk}^2\right) + \sum_{k=1}^{5}\sum_{h=6}^{7} b_{kh}T_{Bk}T_{Bh} \tag{7}$$

where $a_0, a_{ik}(i = 1, 2), b_{kh}$ are coefficients, and T_{Bk}, T_{Bh} are the measured brightness temperatures of channels k and h, respectively. Here, $T_{B1} = T_{B19V}, T_{B2} = T_{B19H}, \ldots, T_{B7} = T_{B85H}$. According to (7) we have transformed the nonlinear problem of the derivation of rain rate from SSM/I data into a linear one, which consists of finding the appropriate values of a_0, a_{ik}, b_{kh}. It is worth noticing that, to avoid using redundant information, among the mixed terms of the second-order polynomial, we have considered only the product between a low-resolution T_{B} and a high-resolution one. In fact, we have analyzed the T_{B} belonging to our database, and we have found that the correlation between the measurements of the low-resolution channels is always greater than 80%. Then, if the channels were included, the noise would have added incoherently, thus reducing the estimation accuracy. The same consideration can be made for the 85-GHz channels, whose correlation reaches 99%.

B. Artificial Neural Network

A retrieval algorithm based on an artificial neural network has been also applied, since it is well known that a multilayer feedforward neural network, having at least one hidden layer, can approximate any nonlinear function relating inputs to outputs. Therefore, the use of powers of $\mathbf{t}_{\mathrm{m}}$ components is not needed, as opposed to linearized regression. If NN represents the neural network function relating input to output, the neural network estimator $\hat{R}_{\mathrm{NN}}$ can be formally expressed as follows:

$$\hat{R}_{\mathrm{NN}} = \mathrm{NN}[\mathbf{t}_m; h]. \tag{8}$$

In (8), h is the number of hidden neurons.

We have chosen a simple architecture consisting of an input layer of seven neurons (i.e., the seven elements of the $\mathbf{t}_{\mathrm{m}}$ vector), one hidden layer of four neurons with tan-sigmoid transfer functions, and an output layer consisting of one neuron (to extract R), with linear transfer functions. The training process is able to produce a network that minimizes the MSE between the output $\hat{R}_{\mathrm{NN}}$ and the true value of R in the training dataset, but the network solution depends on the initialization of the weights and the biases. For the sake of finding the correct weights for the optimum solution, we have generated ten different networks (i.e., we have performed ten training runs with all weights and biases reinitialized), and we have selected the one presenting the minimum MSE. Instead of the standard backpropagation, the Levenberg–Marquardt algorithm [20] with 100 learning cycles has been used for a faster training.

C. MAP Probability Method

Within a Bayesian framework, various approaches can be used to derive an empirical surface rain rate estimator. Here, we consider the MAP probability criterion, which is described in detail in [5] and [15] and summarized, for the sake of completeness, in the Appendix. In this case, the parameter to be estimated is R, and the MAP implementation is based on a binned analysis of the training set as in [10]. The range of the rain rate variability has been divided into N intervals $i\,(i = 1, \ldots, N)$, each 0.2 mm/h wide (the rain gauge resolution), and for each interval the associated T_{B}'s in the training dataset have been averaged. In this way, the mean brightness temperature vector $\langle \mathbf{t}_{\mathrm{m}}(i) \rangle$ for each rain rate bin $R(i)$ has been found. As it is depicted in detail in the Appendix, in this case, the MAP criterion requires maximizing the following function:

$$p(\mathbf{t}_m \mid R)p(R) \tag{9}$$

where $p(\boldsymbol{t}_m \mid R)$ can be determined assuming a multivariate Gaussian distribution around the mean value $\langle \mathbf{t}_{\mathrm{m}}(i) \rangle$ for all $\mathbf{t}_{\mathrm{m}}$ values corresponding to the rain rate bin $R(i)$. As for $p(R)$, there is strong experimental evidence that it is a log-normal probability density function (pdf) [21], [22], and such evidence has been confirmed, for our region of interest as well, by means of a chi-square test [9]. The empirical MAP (EMAP) estimation of R from a radiometric measurement $\mathbf{t}_{\mathrm{m}}$ corresponds (see the

Appendix) to minimize the following function with respect to $R(i)$

$$d_{\mathrm{EMAP}}(\mathbf{t}_{\mathrm{m}}, i) = [\mathbf{t}_{\mathrm{m}} - \langle \mathbf{t}_{\mathrm{m}}(i) \rangle]^{\mathrm{T}} \mathbf{C}_i^{-1} [\mathbf{t}_{\mathrm{m}} - \langle \mathbf{t}_{\mathrm{m}}(i) \rangle] + \ln[\det(\mathbf{C}_i)] + (1/\sigma^2)[\ln(\mathrm{R}(i)) - \mu] + \ln(\sigma^2) + 2\ln(R(i)) \quad (10)$$

where μ and σ are the parameters of the log-normal pdf, $\mathbf{C}_i$ is the covariance matrix of $\mathbf{t}_{\mathrm{m}}$ for the interval $R(i)$ computed from the training dataset and $\det(\mathbf{C}_i)$ is its determinant. Superscripts "T" and "-1" indicate transposition and inversion of a matrix, respectively.

D. Literature Algorithms

Among the class of empirical regression algorithms, the National Oceanic and Atmospheric Administration (NOAA) algorithm for rain retrieval over land is based on the scattering index (SI_L) defined by the following equation [10]:

$$\mathrm{SI}_L = 451.9 - 0.44 T_{B19V} - 1.775 T_{B22V} + 0.005\,75 T_{B22V}^2 - T_{B85V}. \quad (11)$$

Values of $\mathrm{SI}_L > 10$ K generally indicate presence of rain. The estimated precipitation is calculated by using a power law form

$$\hat{R}_{\mathrm{SI}} = a \mathrm{SI}_L^b \quad (12)$$

where $a = 0.036$ and $b = 1.491$ are coefficients derived using coincident SSM/I and radar data.

More recently, the calibration/validation (CV) algorithm for SSM/I has been updated giving rise to the following regression formula [11]:

$$\hat{R}_{\mathrm{CV}} = \exp\left[c_0 + \sum_{k=1}^{N} c_k T_{Bk}\right] - c_{00}. \quad (13)$$

In (13), $c_k (k = 0, \ldots, N)$, and c_{00} are regression coefficients. When 85-GHz channel measurements over land are available, then $N = 2$ with $k = 1$ and $k = 2$ corresponding to 85 V and 85 H channels, respectively, $c_0 = 3.297\,16, c_1 = -0.012\,90, c_2 = 0.008\,77$ and $c_{00} = -8$. Alternatively, if the 85-GHz channels are unavailable, then $N = 2$ with $k = 1$ and $k = 2$ corresponding to 37 V and 19 V channels, respectively, $c_0 = -17.768\,49, c_1 = -0.096\,12, c_2 = 0.156\,78$, and $c_{00} = -1$.

The two-channel (2C) empirical algorithm proposed by Conner and Petty is also considered here. The 2C method simply compares the T_{B} differences at 37 and 85 GHz with those of the background fields, arguing that this difference should contain the precipitation signature only. Its general form is given by [12]

$$\hat{R}_{2C} = d_0 + d_1[(T_{B37V} - T_{B85V}) - \langle (T_{B37V} - T_{B85V}) \rangle] \quad (14)$$

where $\langle (T_{B37V} - T_{B85V}) \rangle$ represents the local monthly means of $T_{B37V} - T_{B85V}$, while $d_0 = -1.3$ and $d_1 = 0.317$.

V. Physical Inversion Techniques

The physical approach introduces an explicit consideration of the vertical distribution of the hydrometeors and of the meteorological variables (temperature, pressure, and humidity), together with a rigorous theoretical treatment of the emission, absorption, and scattering of the radiation through a rainy cloud (the forward model) [4]. This kind of approach has been already described in several works [6], [9], [15], in which a Bayesian estimator of the coarse profile of hydrometeor contents within a precipitating cloud has been introduced. We have adopted a microphysical cloud model, named University of Wisconsin–Non-hydrostatic Modeling System (UW-NMS), which is capable of explicitly describing the vertical distribution of four species of hydrometeors (i.e., cloud droplets, rain drops, graupel particles, and ice particles) [1], [23]. From the original vertical resolution of about 0.5 km, which determines 42 altitude levels, the number of cloud layers has been reduced to at most seven [15]. The modeled cloud vertical structures have been classified into genera and species according to the World Meteorological Organization (WMO) nomenclature, so that they have been inscribed to $N_c = 9$ cloud classes [5]. Each cloud belonging to class c ($c = 1, \ldots, N_c$) is defined by a vector $\mathbf{g}$ whose elements are the equivalent water contents of the various hydrometeors at different altitudes (i.e., cloud layers). In order to associate to each cloud profile its spectral signature, we have used a plane-parallel radiative transfer model (the forward model) based on the Eddington solution [5].

This modeled cloud database has been used to infer the statistics of vector $\mathbf{g}$ within each class needed in the inverse problem. A major issue, which has to be faced when adopting the outputs of a cloud-resolving model, is the discrepancy between the environmental conditions of the simulation (referred to a summer tropical storm, in this case) with respect to the climatology of the considered area at different seasons (e.g., temperature, pressure, and humidity profiles). Such discrepancy may produce a bias in the simulated brightness temperatures with respect to the actual SSM/I measurements, which could lead to remarkable rain estimation errors. Therefore, in determining the statistics of the clouds, it is necessary to match the climatic conditions of the area of interest and their annual variability without loosing the microphysical consistency of the cloud database derived from the model. The matching procedure adopted by the authors is described in [9]. Ground measurements provided by rain gauge networks, data furnished by radiosounding balloons, as well as radiometric observations coming from meteorological satellites (e.g., infrared radiometers) have been used to complement the output of the microphysical cloud model. We have performed the parametric statistical analysis considering all the hydrometeors as Gaussian variables with mean, standard deviation and correlation matrix derived from the UW-NMS model and the matching procedure mentioned above.

The physical inversion techniques described below are all based on a Monte Carlo approach, requiring a statistical gener-

ation of a large number of cloud vectors $\mathbf{g}$ belonging to class c and the corresponding modeled T_{B} vectors (i.e., the radiometric signatures) $\mathbf{t}(\mathbf{g}, c)$ [15]. With respect to previous works, we have increased the number of synthetic cloud profiles giving rise to a database consisting of 12 datasets (one for each month) with $N_{\mathrm{g}} = 1000$ profiles for each of the nine considered cloud classes.

Note that, in order to face the problem of inhomogeneity of the surface background in our Monte Carlo procedure, we have introduced a sort of equivalent emissivity, and we have let the surface emissivity in the database be randomly variable within a given statistics (monthly values, standard deviations, and correlation matrices) derived by analyzing one year of radiometric signatures in clear air, as described in detail in [9]. In this way, since the topography of our area is far from being flat, and the land use is inhomogeneous, the final estimated accuracy is not biased toward too optimistic values.

As mentioned, the MAP criterion has been adopted for inverting the forward model in the previous papers [6], [9], [15]. According to this criterion (see the Appendix for the details), given measurement $\mathbf{t_m}$, the most probable cloud is inferred by finding the pair of c and $\mathbf{g}$, which minimizes the following function:

$$\begin{aligned} d_{\mathrm{MAP}}(\mathbf{t_m}, \mathbf{g}) = & [\mathbf{t_m} - \mathbf{t}(\mathbf{g}, c)]^T \mathbf{C}_{\mathrm{e}}^{-1} [\mathbf{t_m} - \mathbf{t}(\mathbf{g}, c)] \\ & + \ln[\det(\mathbf{C}_{\mathrm{e}})] + (\mathbf{g} - \mathbf{m}_{\mathrm{c}})^T \mathbf{C}_{\mathrm{gc}}^{-1} (\mathbf{g} - \mathbf{m}_{\mathrm{c}}) \\ & - 2 \ln P(c) + \ln[\det(\mathbf{C}_{\mathrm{gc}})] + D_c \ln(2\pi) \end{aligned} \quad (15)$$

where $P(c)$ is the prior probability of class c (that have been assumed all equal in the next section), $\mathbf{C}_{\mathrm{e}}$ is the covariance matrix of the error affecting both the measured T_{B} and the modeled one, $\mathbf{m}_{\mathrm{c}}$ and $\mathbf{C}_{\mathrm{gc}}$ are the mean vector and the covariance matrix of the $\mathbf{g}$ vectors within class c, and D_c is the dimension of these vectors. The latter generally depends on the considered class, and it can be at most equal to 28 (i.e., seven layer by four hydrometeors in each layer). The estimated precipitation is related to the rain density g_1 of the lowest layer of the selected cloud structure through a formulation that accounts for gravity, atmospheric drag, and the fall velocity [24]. The minimization of (15) may be based on optimization techniques that require running the forward model iteratively. For reducing computing time, according to the Monte Carlo approach, the most probable profile $\mathbf{g}$ is searched in the database of vectors $\mathbf{g}$ and the corresponding $\mathbf{t}(\mathbf{g}, c)$ generated once and for all. Note that an apparent discrepancy with Section IV-C concerns the statistic of the parameter to be estimated (Gaussian for $\mathbf{g}$ and log-normal for R). Actually, since the population here is divided in several classes, it can be shown that the statistics of the total sample is not far from being log-normal [9].

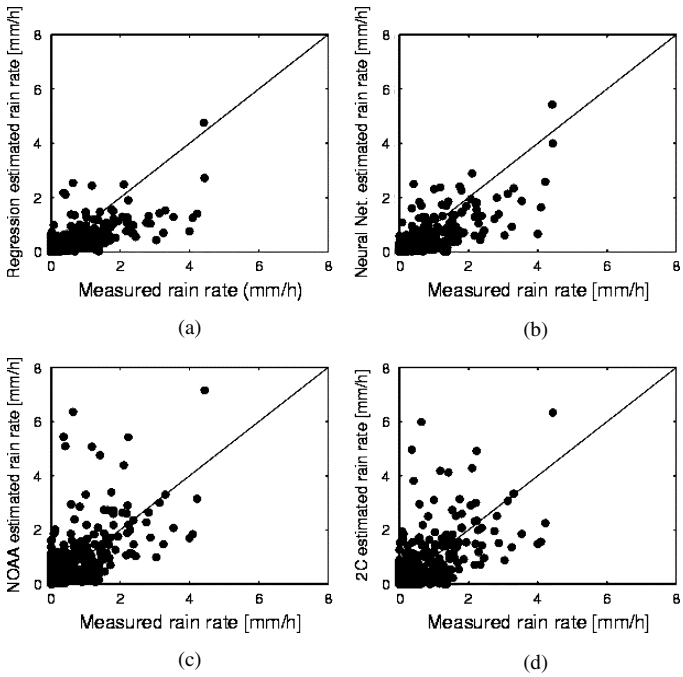

Fig. 7. Comparison between rain gauge measurements over Central Italy at basin level and SSM/I-based estimates of rain rate for the whole validation set obtained by using(a) the neural network, (b) the regression, (c) the NOAA algorithm, and (d) the 2C procedure. The neural network and the regression are trained by using the complete training set.

In this paper, a novel Bayesian scheme is proposed, which is the MMSE. It is described in detail in part B of the Appendix, in which it is demonstrated that the estimated value of g_1, which, as previously mentioned, is related to rain rate, is given by (16), shown at the bottom of the page, where superscript k indicates the kth profile of each class of the database, and a Monte Carlo integration is adopted.

VI. Analysis of the Results

In this section, the behavior of the various retrieval methods is discussed. As mentioned, we have performed two classifications of events, one from rain gauge data and the other from radiometric measurements. The former has been applied to the whole database. It has been used, for the training set, to perform different kinds of training and, for the validation set, to divide it into subsets for the purpose of evaluating the performances of the algorithms for different types of events.

First, we have assessed algorithms that do not make any use of a preliminary discrimination of the type of event (not even rainy or nonrainy conditions). They are the regression and the neural network, both trained on the whole training set and the literature algorithms. The results at basin level (i.e., averaged over the basin) are statistically summarized in Table III in terms of correlation coefficient between measurements and estimates

$$\hat{g}_{1\mathrm{MMSE}} = \frac{\sum_{c=1}^{N_c} P(c) \sum_{k=1}^{Ng} g_1^k \exp\left[-\frac{1}{2}(\mathbf{t}_m - \mathbf{t}(\mathbf{g}^k, c))^T \mathbf{C}_e^{-1} (\mathbf{t}_m - \mathbf{t}(\mathbf{g}^k, c))\right]}{\sum_{c=1}^{N_c} P(c) \sum_{k=1}^{Ng} \exp\left[-\frac{1}{2}(\mathbf{t}_m - \mathbf{t}(\mathbf{g}^k, c))^T \mathbf{C}_e^{-1} (\mathbf{t}_m - \mathbf{t}(\mathbf{g}^k, c))\right]} \quad (16)$$

TABLE III
STATISTICAL COMPARISON BETWEEN THE RAIN RATES MEASURED BY THE RAIN GAUGE NETWORK AT BASIN LEVEL AND THOSE ESTIMATED FROM SSM/I BY USING THE NEURAL NETWORK, THE REGRESSION, THE NOAA ALGORITHM, AND THE 2C ALGORITHM. THE NEURAL NETWORK AND THE REGRESSION ARE TRAINED BY USING THE COMPLETE TRAINING SET. THE COMPARISON IS EXPRESSED IN TERMS OF CORRELATION COEFFICIENT BETWEEN MEASUREMENTS AND ESTIMATES AND ROOT MEAN SQUARE ERROR. THE WHOLE VALIDATION SET AND THE SUBSETS CORRESPONDING TO STRATIFORM AND CONVECTIVE EVENTS ARE CONSIDERED SEPARATELY

		Regression	Neural network	NOAA	2C	CV
Whole dataset	**Correlation coefficient**	0.75	0.79	0.69	0.70	0.32
Whole dataset	**Rms error [mm/h]**	0.25	0.23	0.37	0.33	0.62
Stratiform events	**Correlation coefficient**	0.77	0.77	0.71	0.72	0.39
Stratiform events	**Rms error [mm/h]**	0.26	0.26	0.37	0.35	0.63
Convective events	**Correlation coefficient**	0.64	0.72	0.59	0.59	0.63
Convective events	**Rms error [mm/h]**	0.82	0.73	1.09	1.01	0.82

TABLE IV
STATISTICAL COMPARISON BETWEEN THE RAIN RATES MEASURED BY THE RAIN GAUGE NETWORK AT BASIN LEVEL AND THOSE ESTIMATED FROM SSM/I BY USING THE NEURAL NETWORK, THE REGRESSION, THE EMPIRICAL MAP, THE PHYSICAL MMSE, AND THE PHYSICAL MAP. THE NEURAL NETWORK, THE REGRESSION, AND THE EMPIRICAL MAP ARE TRAINED BY USING ONLY THE SAMPLES OF THE TRAINING SET BELONGING TO RAINY EVENTS. THE COMPARISON IS EXPRESSED IN TERMS OF CORRELATION COEFFICIENT BETWEEN MEASUREMENTS AND ESTIMATES AND ROOT MEAN SQUARE ERROR. THE WHOLE VALIDATION SET AND THE SUBSETS CORRESPONDING TO STRATIFORM AND CONVECTIVE EVENTS ARE CONSIDERED SEPARATELY

		Regression	Neural network	Emp. MAP	Phys. MAP	Phys. MMSE
Whole dataset	**Correlation coefficient**	0.76	0.79	0.67	0.72	0.74
Whole dataset	**Rms error [mm/h]**	0.24	0.23	0.28	0.29	0.28
Stratiform events	**Correlation coefficient**	0.74	0.74	0.63	0.68	0.73
Stratiform events	**Rms error [mm/h]**	0.27	0.27	0.31	0.37	0.35
Convective events	**Correlation coefficient**	0.68	0.73	0.69	0.66	0.68
Convective events	**Rms error [mm/h]**	0.75	0.70	0.77	0.75	0.74

and root mean square (rms) error. The bias error is not reported in this table and in the two successive ones, since it is always very low. In Table III (and successive), different test sets are used, i.e., taking into consideration the whole test set and the two subsets corresponding to stratiform and convective events (according to the rain gauge data). The neural network furnishes the best results, considering both the correlation coefficient and the rms error, for every test set. In particular, its good performance for the whole database demonstrates that it is also fairly able to distinguish between rainy and nonrainy situations. The behavior of the regression is good too and, as expected, the results provided by the proposed algorithms are better than those furnished by literature ones. We have included the information about correlation coefficient also for stratiform events to analyze all the results according to the same statistical parameters, but, in these cases, rain rates are so low that this quantity cannot be considered very meaningful. Fig. 7 shows the comparison between estimates and measurements for the whole validation set for neural network, regression, and for the two literature algorithms, which present the best behavior for our dataset: NOAA and 2C. Note that the precipitation values are low, since we are considering the average of all the rain measurements in the basin of interest. It is evident that there is an overestimation of moderate precipitation presented by NOAA and 2C methods of moderate precipitation. This is the reason for the quite remarkable difference between the rms errors of the proposed algorithms and those of the literature ones, for convective rain (see Table III).

In the previous analysis, we have considered neither the physical procedures nor the empirical MAP (EMAP). The former are based on statistical assumptions which imply the presence of a precipitating cloud, whereas EMAP is based on the log-normal distribution of R, which can be applied for rainy conditions only. Therefore these methods must be preceded by a screening procedure so that we applied them only to SSM/I data belonging to events considered rainy (i.e., stratiform or convective) by the classification based on radiometric measurements described in the previous section. As for the regression and the neural network, in this case, they have been trained on the subset corresponding to rainy events. The results are presented in Table IV. The performances of the neural network and regression are substantially the same with respect to the previous case, thus confirming their capability to discriminate rainy situations if trained on the entire database. The small increase of rms error for stratiform events (0.27 mm/h instead of 0.26 mm/h) is balanced by the decrease of this error for convective ones (0.75 mm/h instead of 0.82 mm/h for the regression method). Among all the developed procedures, the EMAP furnishes the worst performances.

As mentioned, one of the objectives of this paper is to confirm the validity of the physical techniques. Their behavior is generally slightly worse than that presented by the neural network, but better than the one provided by literature algorithms especially if intense convective rain is considered. It is worth noticing that the matching of the simulations to the climatic conditions of the Mediterranean area described in [9] has been necessary to achieve the performances provided by the physical methods. The procedure suggests complementing the fundamental information provided by a cloud model through the addition of statistics characterizing cloudy systems occurring in the area of interest. It is unrealistic to increase the representativeness of the simulations by using a number of different cloud resolving model runs suitable to span a significant range of both precipitation types and seasonal conditions, as well as, obviously, to develop an empirical method for every climatic region. Our approach could represent a strategy to use microwave radiometric data for rain rate retrieval in the mesoscale range, since it implicitly foresees an extension to different geograph-

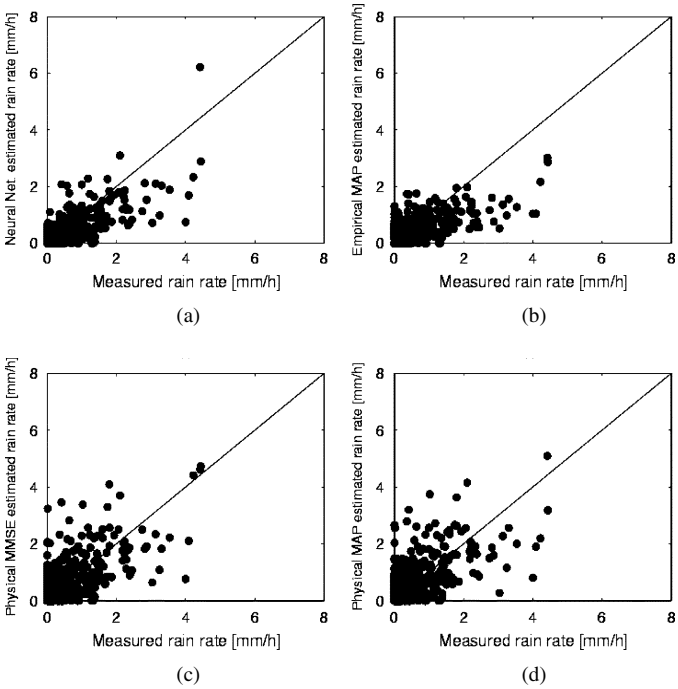

Fig. 8. Comparison between rain gauge measurements over Central Italy at basin level and SSM/I-based estimates of rain rate for the whole validation set obtained by using (a) the neural network, (b) the empirical MAP, (c) the physical MMSE, and (d) the physical MAP. The neural network and the empirical MAP are trained by using only the samples of the training set belonging to rainy events.

ical zones, provided the availability of local meteorological parameters (which can be furnished by radiosounding balloons, meteorological analyses, as well as radiometric observations coming from meteorological satellites).

Fig. 8 shows the comparison between measurements and estimates provided by the two physical procedures and by the EMAP. Neural network estimates obtained by training it on the subset consisting of only rainy events are also considered as benchmarks. It can be observed that moderate precipitation is fairly well estimated with respect to literature methods.

The complete classification provided by the screening technique described in Section III-B can be used for the purpose of further improving the retrieval capability of the empirical methods. Therefore, we have derived different neural networks and regression coefficients, together with different mean vector and covariance matrices for the EMAP, for the stratiform and convective events included in the training set. Table V reports the results. The correlation coefficient between measurements and neural network estimates reaches 81% for the whole validation set, thus confirming that with a specialized training it is possible to improve the performances of the empirical techniques. The improvement is meaningful for high convective rain, for which the rms error presents a minimum of 0.66 mm/h, and the correlation is 0.77 for the neural network, while with the training on the whole dataset, the corresponding values are 0.73 and 0.72 mm/h, respectively (see Table III). Such improvement appears evident also by observing Fig. 9, in which a comparison between estimates and measurements for neural network and regression is illustrated and by comparing it with the top panels of Fig. 7.

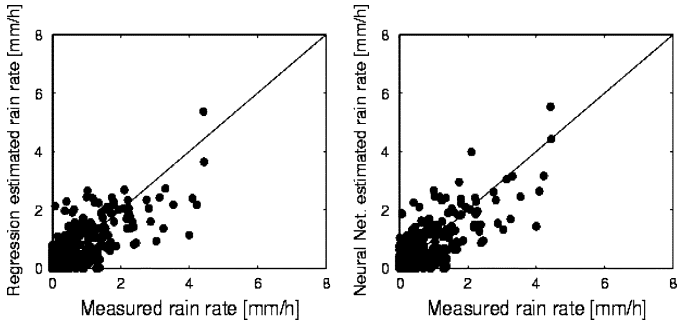

Fig. 9. Comparison between rain gauge measurements over Central Italy at basin level and SSM/I-based estimates of rain rate for the whole validation set obtained by using (a) the neural network and (b) the regression trained by considering separately the stratiform and convective events belonging to the training set.

Although the results at pixel level have to be considered with caution, a mention of the rms estimation error, as far as rain gauges detecting rain are concerned, can be meaningful. It is confirmed that the neural network provides the best results. If it is trained on the whole database and tested on the rainy pixels (according to the rain gauges), its rms error is equal to 2.9 mm/h. The physical algorithms give an rms error of 3.0 (MMSE) and 3.2 mm/h (MAP). The comparison with literature algorithms remains satisfactory, since both NOAA and 2C provide an rms error equal to 3.3 and 4.1 mm/h, respectively. Note that the estimates at pixel level always show low correlation coefficient with measurements and underestimate high rain rates, probably because of the smoothing effect due to the poor geometric resolution of the radiometer.

VII. Conclusion

A large database of colocated SSM/I and rain gauge measurements relative to the Mediterranean region has been set up in order to carry out an intercomparison of some retrieval techniques based both on physical and empirical approaches. To ensure the reliability of such dataset, nine years of data have been considered, and a preliminary quality control has been performed. The expected improvement of the retrieval capability with respect to algorithms developed for global-scale applications has been observed, especially for high rain rates. Among the five proposed inversion techniques, the neural network trained on an experimental dataset has furnished the best results. The various techniques have been tested with different kinds of precipitation, classified according to some statistical parameters inferred from rain gauge measurements, and it has been verified that it is possible to improve significantly the ability of the empirical techniques to detect intense rain by training them in convective events only.

However, this paper has assessed the validity of the physically based retrieval adopted in previous works, which incorporates also a tuning procedure to the climatic conditions of the geographical area of interest based on the addition, to a cloud resolving model, of further information characterizing cloudy systems occurring in the same region. This allows one to relax the link with the original mesoscale simulation which

TABLE V
STATISTICAL COMPARISON BETWEEN THE RAIN RATES MEASURED BY THE RAIN GAUGE NETWORK AT BASIN LEVEL AND THOSE ESTIMATED FROM SSM/I BY USING THE NEURAL NETWORK, THE REGRESSION, AND THE EMPIRICAL MAP TRAINED BY CONSIDERING SEPARATELY THE STRATIFORM AND CONVECTIVE EVENTS BELONGING TO THE TRAINING SET. THE COMPARISON IS EXPRESSED IN TERMS OF CORRELATION COEFFICIENT BETWEEN MEASUREMENTS AND ESTIMATES AND ROOT MEAN SQUARE. THE WHOLE VALIDATION SET AND THE SUBSETS CORRESPONDING TO STRATIFORM AND CONVECTIVE EVENTS ARE CONSIDERED SEPARATELY

		Regression	Neural network	Emp. MAP
Whole dataset	**Correlation coefficient**	0.79	0.81	0.66
Whole dataset	**Rms error [mm/h]**	0.23	0.22	0.29
Stratiform events	**Correlation coefficient**	0.66	0.67	0.56
Stratiform events	**Rms error [mm/h]**	0.28	0.26	0.29
Convective events	**Correlation coefficient**	0.75	0.77	0.70
Convective events	**Rms error [mm/h]**	0.68	0.66	0.80

concerns a specific rainy event, but, at the same time, to preserve the original microphysics. We have shown that the MAP method and, in particular, the minimum mean square estimator provide results which are quite similar to those given by empirical methods calibrated on the region of interest and better than the ones furnished by literature algorithms, thus demonstrating the potentiality of our physical-statistical approach to retrieve precipitation intensity from spaceborne microwave radiometric data, over a limited geographical area. This approach is certainly less demanding in terms of modeled data and ground truth with respect to purely physical and purely empirical approaches, respectively. The methodology is inherently designed for matching local area conditions, and we trust it is suitable for other locations. We have demonstrated the validity of this methodology in our region of interest, but this does not represent a conclusive statement, since the final choice will certainly require a case-by-case tradeoff in terms of availability of data and models, as well as implementation costs. For global-scale retrieval, which is not the object of our work, the knowledge of the minimum number of climatological adaptations should be further investigated.

APPENDIX

The detailed description of the Bayesian MAP criterion is furnished in [9]. However, for the sake of clarity and completeness, in the following its main steps are summarized. Moreover, the novel MMSE is introduced.

A. MAP Probability Method

Generally, the Bayesian approach to the estimation of a parameter θ, starting from a vector of measurements $\mathbf{y}$, is based on the definition, for each pair $(\theta, \hat{\theta})$ ($\hat{\theta}$ represents the estimate of $\theta : \hat{\theta} = f(\mathbf{y})$), of a cost $c(\theta, \hat{\theta}) \geq 0$ [25]. The objective is the minimization of the expected value of the cost, which is named risk r and is given by

$$r = E\{c(\hat{\theta}, \hat{\theta})\} = \int \int c(\hat{\theta}, \hat{\theta}) p(\hat{\theta}, \mathbf{y}) d\hat{\theta} d\mathbf{y}. \tag{17}$$

The MAP criterion assumes that the cost is uniform

$$c(\hat{\theta}, \hat{\theta}) = \begin{cases} 0, & -a/2 \leq \hat{\theta} - \theta \leq a/2 \quad a \to 0 \\ 1, & \text{otherwise.} \end{cases} \tag{18}$$

The corresponding risk is given by

$$r(\mathrm{MAP}) = \int d\mathbf{y} \left[\int_{-\infty}^{\hat{\theta}-a/2} p(\hat{\theta}, \mathbf{y}) d\hat{\theta} + \int_{\hat{\theta}+a/2}^{+\infty} p(\hat{\theta}, \mathbf{y}) d\hat{\theta} \right]. \tag{19}$$

Since, for the Bayes theorem, $p(\theta, \mathbf{y}) = p(\theta \,|\, \mathbf{y}) p(y)$, and the unlimited integral of $p(\theta \,|\, \mathbf{y})$ is 1, then (19) becomes [25]

$$r(\mathrm{MAP}) = \int p(\mathbf{y}) dy \left[1 - \int_{\hat{\theta}-a/2}^{\hat{\theta}+a/2} p(\hat{\theta} \,|\, \mathbf{y}) d\hat{\theta} \right]. \tag{20}$$

Consequently, the MAP criterion requires to search for the parameter θ that minimizes the conditioned *a posteriori* probability $p(\theta \,|\, \mathbf{y})$ of θ given the observation $\mathbf{y}$.

In our case, $\mathbf{y}$ is represented by the multifrequency T_{B} vecor $\mathbf{t_m}$. The Bayes theorem prescribes that

$$p(\theta \,|\, \mathbf{t}_m) = \frac{p(\mathbf{t}_m \,|\, \theta) p(\theta)}{p(\mathbf{t}_m)}. \tag{21}$$

In (21), $p(\mathbf{t}_{\mathrm{m}})$ represents a constant term when the measurement is known and can be neglected. In the case of the empirical MAP (Section IV-C), θ coincides with rain rate R. As mentioned, we have carried out a binned analysis of the range of the rain rate variability, and $p(\mathbf{t}_{\mathrm{m}} \,|\, R)$ can be determined by assuming a multivariate Gaussian distribution for every $\mathbf{t}_{\mathrm{m}}$ corresponding to the generic bin $R(i)$, characterized by a mean vector $\langle \mathbf{t}_{\mathrm{m}}(i) \rangle$ and by a covariance matrix $\mathbf{C}_{\mathrm{i}}$

$$p(\mathbf{t}_{\mathrm{m}} \,|\, R) = \frac{1}{(2\pi)^{7/2} \sqrt{\det(\mathbf{C}_{\mathrm{i}})}} \cdot \exp\left[-\frac{1}{2} (\mathbf{t}_{\mathrm{m}} - \langle \mathbf{t}_{\mathrm{m}}(i) \rangle)^{\mathrm{T}} \mathbf{C}_i^{-1} (\mathbf{t}_{\mathrm{m}} - \langle \mathbf{t}_{\mathrm{m}}(i) \rangle) \right] \tag{22}$$

where 7 is the dimension of $\mathbf{t}_{\mathrm{m}}$, $\det(\cdot)$ indicates determinant, and superscripts "T" and "-1" indicate transposition and inversion of a matrix, respectively.

Since $p(R)$ can be considered a log-normal pdf, it is assumed that

$$p(R) = \frac{\exp\{-[\ln(R) - \mu]^2 / (2\sigma^2)\}}{R\sqrt{2\pi\sigma^2}}, \qquad R > 0. \tag{23}$$

In (23), μ and σ are the parameters of the log-normal distribution, obtained by best fitting the rain rate histogram in the training dataset. By computing the natural logarithms, the empirical MAP (EMAP) estimation of R from a radiometric measurement $\mathbf{t}_\mathrm{m}$ is equivalent to minimizing the following function with respect to $R(i)$:

$$d_{\mathrm{EMAP}}(\mathbf{t}_\mathrm{m}, i) = [\mathbf{t}_\mathrm{m} - \langle \mathbf{t}_\mathrm{m}(i)\rangle]^\mathrm{T}\mathbf{C}_i^{-1}[\mathbf{t}_\mathrm{m} - \langle \mathbf{t}_\mathrm{m}(i)\rangle] + \ln[\det(\mathbf{C}_i)] + (1/\sigma^2)[\ln(R(i)) - \mu] + \ln(\sigma^2) + 2\ln(R(i)). \quad (24)$$

As far as the physical MAP is concerned (Section V), the whole cloud profile $\mathbf{g}$ is estimated, and the probability density function $p(\mathbf{g}, c\,|\,\mathbf{t}_m)$, which is proportional to $p(\mathbf{t}_\mathrm{m}\,|\,\mathbf{g}, c)p(\mathbf{g}\,|\,c)P(c)$, has to be maximized ($c$ represents the class and $P(c)$ the probability of occurrence of c, considered the same for all the classes). Since we have assumed $\mathbf{g}$ as a Gaussian random vector within each class, the following applies for $p(\mathbf{g}\,|\,c)$:

$$p(\mathbf{g}\,|\,c) = \frac{1}{(2\pi)^{D_c/2}\sqrt{\det(\mathbf{C}_\mathrm{gc})}} \cdot \exp\left[-\frac{1}{2}(\mathbf{g} - \mathbf{m}_\mathrm{c})^\mathrm{T}\mathbf{C}_\mathrm{gc}^{-1}(\mathbf{g} - \mathbf{m_c})\right] \quad (25)$$

where $\mathbf{m}_\mathrm{c}$ and $\mathbf{C}_\mathrm{gc}$ are the mean vector and the covariance matrix of the $\mathbf{g}$ vectors within class c, and D_c is the dimension of these vectors.

As for $p(\mathbf{t_m}\,|\,\mathbf{g}, c)$, its distribution is originated either from radiometer errors and from model errors. It has been assumed Gaussian too, with mean value equal to the modeled T_B vector $\mathbf{t}(\mathbf{g}, c)$, associated to the cloud vector $\mathbf{g}$ within class c by the forward model and covariance matrix $\mathbf{C}_\mathrm{e}$

$$p(\mathbf{t_m}\,|\,\mathbf{g}, c) = \frac{1}{(2\pi)^{7/2}\sqrt{\det(\mathbf{C}_\mathrm{e})}} \cdot \exp\left[-\frac{1}{2}(\mathbf{t_m} - \mathbf{t}(\mathbf{g}, c))^\mathrm{T}\mathbf{C_e}^{-1}(\mathbf{t_m} - \mathbf{t}(\mathbf{g}, c))\right]. \quad (26)$$

If the natural logarithms are computed, it can be demonstrated, with some mathematical arrangements [15], that the most probable profile $\mathbf{g}$ of a cloud belonging to class c is inferred by searching the cloud class c and the profile $\mathbf{g}$, which minimize the following function:

$$d_{\mathrm{MAP}}(\mathbf{t_m}, \mathbf{g}) = [\mathbf{t_m} - \mathbf{t}(\mathbf{g}, c)]^T\mathbf{C}_\mathrm{e}^{-1}[\mathbf{t_m} - \mathbf{t}(\mathbf{g}, c)] + \ln[\det(\mathbf{C}_\mathrm{e})] + (\mathbf{g} - \mathbf{m}_\mathrm{c})^T\mathbf{C}_\mathrm{gc}^{-1}(\mathbf{g} - \mathbf{m}_\mathrm{c}) - 2\ln P(c) + \ln[\det(\mathbf{C}_\mathrm{gc})] + D_c\ln(2\pi). \quad (27)$$

B. Minimum Mean Square Estimator

As opposed to MAP, which considers a uniform error function, the MMSE minimizes the risk for a squared error. In this case, the parameter to be estimated is g_1 and, indicated with $\hat{g}_{1\mathrm{MMSE}}$ its estimator, the risk function r is given by [25]

$$r(\mathrm{MMSE}) = \int_0^\infty p(\mathbf{t}_m)d\mathbf{t}_m \left\{\int_0^\infty (g_1 - \hat{g}_{1\mathrm{MMSE}})^2 p(g_1\,|\,\mathbf{t}_m)dg_1\right\}. \quad (28)$$

Since $p(\mathbf{t_m})$ is nonnegative, it is required to minimize the quantity in bracket. It can be demonstrated [26] that the following MMSE estimator is obtained for the equivalent water content of the hydrometeor rain in the lowest level:

$$\hat{g}_{1\mathrm{MMSE}} = \int_0^\infty g_1 p(g_1\,|\,\mathbf{t}_m)dg_1. \quad (29)$$

It can be observed that the estimate corresponds to the expected value of g_1 given the measurement $\mathbf{t_m}$. Note that $p(g_1\,|\,\mathbf{t_m})$ can be expressed as function of $p(\mathbf{g}, c\,|\,\mathbf{t_m})$ by saturating with respect to all the variables, except g_1 (i.e., the continuous variables $\mathrm{g}_2 \ldots \mathrm{g}_\mathrm{D}$ and the discrete variable c) so that the following applies:

$$p(g_1\,|\,\mathbf{t}_m) = \sum_{c=1}^{N_c}\int_0^\infty \cdots \int_0^\infty p(\mathbf{g}, c\,|\,\mathbf{t}_m)dg_2 \ldots dg_{D_c}. \quad (30)$$

By substituting (30) in (29), the MMSE estimator can be written as

$$\hat{g}_{1\mathrm{MMSE}} = \sum_{c=1}^{N_c}\int_0^\infty \cdots \int_0^\infty g_1 p(\mathbf{g}, c\,|\,\mathbf{t}_m)dg_1dg_2 \ldots dg_{D_c}. \quad (31)$$

According to the Bayes theorem, $p(\mathbf{g}, c\,|\,\mathbf{t_m})$ is given by the following equation:

$$\begin{aligned} p(\mathbf{g}, c, \mathbf{t}_m) &= p(\mathbf{g}, c\,|\,\mathbf{t}_m)p(\mathbf{t}_m) \\ &= p(\mathbf{t}_m\,|\,\mathbf{g}, c)p(\mathbf{g}, c) \\ &= p(\mathbf{t}_m\,|\,\mathbf{g}, c)p(\mathbf{g}\,|\,c)P(c). \end{aligned} \quad (32)$$

As mentioned, both $p(\mathbf{g}\,|\,c)$ and $\mathrm{p}(\mathbf{t_m}\,|\,\mathbf{g}, c)$ have been considered as Gaussian random variables, whereas $\mathrm{p}(\mathbf{t_m})$ can be obtained by saturating (32) with respect to the continuous random variable $\mathbf{g}$ and with respect to the discrete one c

$$p(\mathbf{t}_m) = \sum_{c=1}^{N_c} P(c)\int_0^\infty \cdots \int_0^\infty p(\mathbf{t}_m\,|\,\mathbf{g}, c)p(\mathbf{g}\,|\,c)dg_1 \cdots dg_{D_c}. \quad (33)$$

By substituting (33) in (32) and $p(\mathbf{g}, c\,|\,\mathbf{t}_m)$ derived from (32) in (31), the MMSE estimator (i.e., the expected value of g_1) can be written as

$$\hat{g}_{1\mathrm{MMSE}} = \frac{\sum_{c=1}^{N_c} P(c)\int_0^\infty \cdots \int_0^\infty g_1 p(\mathbf{t}_m\,|\,\mathbf{g}, c)p(\mathbf{g}\,|\,c)dg_1 \cdots dg_{D_c}}{\sum_{c=1}^{N_c} P(c)\int_0^\infty \cdots \int_0^\infty p(\mathbf{t}_m\,|\,\mathbf{g}, c)p(\mathbf{g}\,|\,c)dg_1 \cdots dg_{D_c}}. \quad (34)$$

The evaluation of the integrals in (34) is a crucial point of this estimation technique. In [2] and [7], the expected value of the parameter to be estimated (the entire profile of a cloud) is similarly considered, but the computation of the integral uses the profiles in the modeled database. Here, we use a different procedure, in which a Monte Carlo integration is applied [27]. The application is based on the generation of N_g profiles for each synthetic class having a Gaussian statistical distribution ($N_g = 1000$, in this case). According to the Monte Carlo method, the

$$\hat{g}_{1\mathrm{MMSE}} = \frac{\sum_{c=1}^{N_c} P(c) \sum_{k=1}^{N_g} g_1^k \exp\left[-\frac{1}{2}(\mathbf{t}_m - \mathbf{t}(\mathbf{g}^k, c))^T \mathbf{C}_e^{-1} (\mathbf{t}_m - \mathbf{t}(\mathbf{g}^k, c))\right]}{\sum_{c=1}^{N_c} P(c) \sum_{k=1}^{N_g} \exp\left[-\frac{1}{2}(\mathbf{t}_m - \mathbf{t}(\mathbf{g}^k, c))^T \mathbf{C}_e^{-1} (\mathbf{t}_m - \mathbf{t}(\mathbf{g}^k, c))\right]} \tag{36}$$

integral of any function $f(\mathbf{g})$ can be approximated by the arithmetic mean of $f(\mathbf{g})/p(\mathbf{g})$ over the N_g samples, in which $p(\mathbf{g})$ is the statistical distribution of $\mathbf{g}$. The (34) can be therefore approximated by

$$\begin{aligned}\hat{g}_{1\mathrm{MMSE}} &= \frac{\sum_{c=1}^{N_c} P(c) \frac{1}{N_g} \sum_{k=1}^{N_g} g_1^k p(\mathbf{t}_m \mid \mathbf{g}^k, c) p(\mathbf{g}^k \mid c)/p(\mathbf{g}^k \mid c)}{\sum_{c=1}^{N_c} P(c) \frac{1}{N_g} \sum_{k=1}^{N_g} p(\mathbf{t}_m \mid \mathbf{g}^k, c) p(\mathbf{g}^k \mid c)/p(\mathbf{g}^k \mid c)} \\ &= \frac{\sum_{c=1}^{N_c} P(c) \sum_{k=1}^{N_g} g_1^k p(\mathbf{t}_m \mid \mathbf{g}^k, c)}{\sum_{c=1}^{N_c} P(c) \sum_{k=1}^{N_g} p(\mathbf{t}_m \mid \mathbf{g}^k, c)} \end{aligned} \tag{35}$$

where superscript k indicates the kth profile generated in the class.

Finally, by substituting (26) in (35), we obtain the expression of our MMSE estimator as in (36), shown at the top of the page.

ACKNOWLEDGMENT

The rain gauge data have been furnished by the *Dipartimento per i Servizi Tecnici Nazionali, Servizio Idrografico e Mareografico Nazionale, Ufficio di Roma*. The SSM/I data have been provided by NOAA/NESDIS, NOAA/FNMOC, GHRC, and SAA. The authors would like to thank the reviewers for providing suggestions and comments that helped to improve the clarity and the completeness of the paper.

REFERENCES

[1] E. A. Smith, A. Mugnai, H. J. Cooper, G. J. Tripoli, and X. Xiang, "Foundations for statistical-physical precipitation retrieval from passive microwave satellite measurements. Part I: Brightness-temperature properties of a time-dependent cloud-radiation model," *J. Appl. Meteorol.*, vol. 31, pp. 506–531, 1992.

[2] C. Kummerow, W. S. Olson, and L. Giglio, "A simplified scheme for obtaining precipitation and vertical hydrometeor profiles from passive microwave sensors," *IEEE Tran. Geosci. Remote Sensing*, vol. 34, pp. 1213–1232, Sept. 1996.

[3] J. Turk, F. S. Marzano, and A. Mugnai, "Effects of degraded sensor resolution upon passive microwave precipitation retrievals of tropical rainfall," *J. Atmos. Sci.*, vol. 55, pp. 1689–1706, 1998.

[4] G. W. Petty, "The status of satellite-based rainfall estimation over land," *Remote Sens. Environ.*, vol. 51, pp. 125–137, 1995.

[5] G. d'Auria, F. S. Marzano, N. Pierdicca, R. Pinna Nossai, P. Basili, and P. Ciotti, "Remotely sensing cloud properties from microwave radiometric observations by using a modeled cloud data base," *Radio Sci.*, vol. 33, pp. 369–392, 1998.

[6] F. S. Marzano, A. Mugnai, G. Panegrossi, N. Pierdicca, E. A. Smith, and J. Turk, "Bayesian estimation of precipitating cloud parameters from combined measurements of spaceborne microwave radiometer and radar," *IEEE Trans. Geosci. Remote Sens.*, vol. 37, pp. 596–613, Jan. 1999.

[7] C. Kummerow, Y. Hong, W. S. Olson, S. Yang, R. F. Adler, J. McCollum, R. Ferraro, G. Petty, D.-B. Shin, and T. T. Wilheit, "The evolution of the Goddard profiling algorithm (GPROF) for rainfall estimation from passive microwave sensors," *J. Appl. Meteorol.*, vol. 40, pp. 1801–1820, 2001.

[8] G. Panegrossi, S. Dietrich, F. S. Marzano, A. Mugnai, E. A. Smith, X. Xiang, G. J. Tripoli, P. K. Wang, and J. P. V. P. Baptista, "Use of cloud model microphysics for passive microwave-based precipitation retrieval: Significance of consistency between model and measurement manifolds," *J. Atmos. Sci.*, vol. 55, pp. 1644–1673, 1998.

[9] L. Pulvirenti, N. Pierdicca, F. S. Marzano, P. Castracane, and G. d'Auria, "A physical-statistical approach to match passive microwave retrieval of rainfall to Mediterranean climatology," *IEEE Trans. Geosci. Remote Sensing*, vol. 40, pp. 2271–2284, Oct. 2002.

[10] R. R. Ferraro and G. F. Marks, "The development of SSM/I rain-rate retrieval algorithms using ground-based radar measurements," *J. Atmos. Ocean. Technol.*, vol. 12, pp. 755–772, 1995.

[11] W. Berg, W. Olson, R. Ferraro, S. J. Goodman, and F. J. LaFontaine, "An assessment of the first- and second-generation navy operational and precipitation retrieval algorithms," *J. Atmos. Sci.*, vol. 55, pp. 1558–1575, 1998.

[12] M. D. Conner and G. W. Petty, "Validation and intercomparison of SSM/I rain-rate retrieval methods over the continental United States," *J. Appl. Meteorol.*, vol. 37, pp. 679–700, 1998.

[13] G. W. Petty and K. B. Katsaros, "Nimbus-7 SMMR precipitation observations calibrated against surface radar during TAMEX," *J. Appl. Meteorol.*, vol. 31, pp. 489–505, 1992.

[14] M. Kitchen and P. M. Jackson, "Weather radar performance at long range—Simulated and observed," *J. Appl. Meteorol.*, vol. 32, pp. 975–985, 1993.

[15] N. Pierdicca, F. S. Marzano, G. d'Auria, P. Basili, P. Ciotti, and A. Mugnai, "Precipitation retrieval from spaceborne microwave radiometers using maximum a posteriori probability estimation," *IEEE Trans. Geosci. Remote Sensing*, vol. 34, pp. 831–846, July 1996.

[16] P. Hollinger, J. L. Peirce, and G. A. Poe, "SSM/I instrument evaluation," *IEEE Trans. Geosci. Remote Sensing*, vol. 28, pp. 781–790, Sept. 1990.

[17] J. T. Tou and R. C. Gonzalez, *Pattern Recognition Principles*. Reading, MA: Addison-Wesley, 1974.

[18] Y. Hong, C. Kummerow, and W. S. Olson, "Separation of convective/stratiform precipitation using microwave brightness temperature," *J. Appl. Meteorol.*, vol. 38, pp. 1195–1213, 1999.

[19] W. S. Olson, Y. Hong, C. Kummerow, and J. Turk, "A texture-polarization method for estimating convective-stratiform precipitation area coverage from passive microwave radiometer data," *J. Appl. Meteorol.*, vol. 40, pp. 1577–1591, 2001.

[20] M. T. Hagan and M. Menhaj, "Training feedforward networks with the Marquardt algorithm," *IEEE Trans. Neural Networks*, vol. 5, pp. 989–993, Nov. 1994.

[21] B. Kedem, H. Pavlopoulos, X. Guan, and D. A. Short, "A probability distribution model for rain-rate," *J. Appl. Meteorol.*, vol. 33, pp. 1486–1493, 1994.

[22] L. LI, Y. Zhu, and B. Zhao, "Rain-rate distributions for China from hourly rain gauge data," *Radio Sci.*, vol. 33, pp. 553–564, 1998.

[23] G. J. Tripoli, "A nonhydrostatic model designed to simulate scale interaction," *Mon. Weather Rev.*, vol. 117, pp. 1342–1359, 1992.

[24] A. Mugnai, E. A. Smith, and G. J. Tripoli, "Foundations for statistical-physical precipitation retrieval from passive microwave satellite measurements. Part II: Emission source and generalized weighting function properties of a time-dependent cloud-radiation model," *J. Appl. Meteorol.*, vol. 32, pp. 17–39, 1993.

[25] N. Pierdicca, "Bayesian techniques in remote sensing," in *Remote Sensing of Atmosphere and Ocean from Space: Models, Instruments and Techniques*. Amsterdam, The Netherlands: Kluwer, 2002, pp. 49–64.

[26] M. Barkat, *Signal Detection and Estimation*. Norwod, MA: Artech House, 1991.

[27] M. H. Kalos and P. A. Whitlock, *Monte Carlo Methods*. New York: Wiley, 1986.

Nazzareno Pierdicca (M'04) was born in Rome, Italy, on June 11, 1954. He received the laurea (Doctor) degree (cum laude) in electronic engineering from the University of Rome "La Sapienza," Rome, Italy, in 1981.

He is currently an Associate Professor in the Faculty of Engineering, University "La Sapienza" and teaches remote sensing and antennas. From 1978 to 1982, he was with the Italian Agency for Alternative Energy (ENEA), performing research and development activities in the field of thermal and mechanical behavior of the nuclear fuel rod. From 1982 to 1990, he worked with Telespazio, Rome, in the Remote Sensing Division. He was involved in and responsible for various projects concerning remote sensing applications, data interpretation, and ground segment design. He was Principal Investigator of the ESA/JRC Agrisar'86 airborne campaign and Co-Investigator of the X-SAR/SIR-C experiment. In November 1990, he joined the Department of Electronic Engineering, University "La Sapienza." His research interests mainly concern electromagnetic scattering models, microwave radiometry of the atmosphere, and SAR land applications. He has been Investigator of the MAC Europe'91 and X-SAR/SIR-C experiments. He is responsible for projects on the above topics funded by the Italian and the European Space Agency.

Dr. Pierdicca is a member of the IEEE Geoscience and Remote Sensing Society (GRSS), of the "Associazione Italiana di Telerilevamento" (AIT), and of "Centro di Telerilevamento a Microonde" (CeTeM).

Luca Pulvirenti received the laurea degree in electronic engineering and the Ph.D. degree in electromagnetism from the University of Rome "La Sapienza," Rome, Italy, in 1999 and 2004, respectively.

He is currently a Post-Doc Researcher in the Department of Electronic Engineering, University "La Sapienza." His research interests include microwave remote sensing of the atmosphere and the earth's surface.

Frank Silvio Marzano (S'89–M'99–SM'03) received the laurea degree (cum laude) in electrical engineering and the Ph.D. degree in applied electromagnetics, in 1988 and 1993, respectively, both from the University or Rome "La Sapienza," Rome, Italy.

He currently teaches a course on antennas and propagation and coordinates the satellite and radar remote sensing group within the Center of Excellence CETEMPS in the Department of Electrical Engineering, University of L'Aquila, L'Aquila, Italy. In 1993, he collaborated with the Institute of Atmospheric Physics (CNR), Rome. From 1994 until 1996, he was with the Italian Space Agency, Rome, as a Post-Doctorate Researcher. After being a Lecturer at the University of Perugia, Perugia, Italy, in 1997, he joined the Department of Electrical Engineering, University of L'Aquila. His current research interests are passive and active remote sensing of the atmosphere from ground-based, airborne, and spaceborne platforms, with a particular focus on precipitation using microwave and infrared data, development of inversion methods, radiative-transfer modeling of scattering media, and scintillation and rain-fading analysis along satellite microwave links.

Dr. Marzano received the Young Scientist Award of the XXIV General Assembly of the International Union of Radio Science in 1993. In 1998, he was the recipient of the Alan Berman Publication Award from the Naval Research Laboratory, Washington, DC. Since 2001, he is the Italian National Delegate for the European COST actions number 720 on meteorological remote sensing and number 280 on satellite communications. He is an Associate Editor for IEEE GEOSCIENCE AND REMOTE SENSING LETTERS.

Piero Ciotti (M'94) received the laurea (Doctor) degree (cum laude) in electronic engineering from the University of Rome "La Sapienza," Rome, Italy, in 1977.

Since 1991, he has been with the Department of Electrical Engineering, University of L'Aquila, L'Aquila, Italy, where he has taught courses on signal theory, electromagnetic fields, and electromagnetic wave propagation. He joined the Department of Electronic Engineering, University "La Sapienza," Rome, in 1977, where he served first as an Assistant Professor and, since 1987, as an Associate Professor, teaching a course on remote sensing. In April 2000, he became a Full Professor of electromagnetics at the same university. During 1984–1985, he conducted research at the Wave Propagation Laboratory, Environmental Research Labotatory, National Oceanic and Atmospheric Administration, Boulder, CO, on a NATO/CNR fellowship. He was a member of the ESA Calibration Team for the ERS-1 Radar Altimeter and a Principal Investigator of the ESA/JRC MAESTRO airborne SAR campaign. He is also Principal Investigator of an ESA/ENVISAT accepted research proposal and member of RA-2/MWR, MERIS, MIPAS, GOMOS, and SCIAMACHY Validation Teams. His research activity has been concerned with microwave remote sensing of the environment, microwave and millimeter-wave atmosphere, microwave line-of-sight propagation, inverse electromagnetic problems, and digital signal processing.

Patrizia Basili (M'97) was born in Rome, Italy, on March 17, 1947. She received the laurea (Doctor) degree in electronic engineering from the University of Rome, Rome, Italy, in 1972.

In 1973, she joined the Department of Electronic Engineering, University of Rome, where she taught courses on electromagnetic fields. She is currently a Full Professor at the Institute of Electronics, University of Perugia, Perugia, Italy, and teaches a course on remote sensing and another on electromagnetic fields. She has also taught courses on electromagnetic wave theory (Calabria University, 1977) and antennas and propagation (Ancona University, 1978–1980). Her research activity has been concerned with microwave and millimeter-wave propagation in the atmosphere, atmospheric remote sensing by radiometry, and inverse problems in electromagnetics.

Giovanni d'Auria was born in Rome, Italy, on June 23, 1931. He received the degree in electrical engineering and the Libera Docenza degree from the University of Rome "La Sapienza" in 1956 and 1964, respectively.

He served in the Italian Air Force, working in the ITAV Laboratories. He was then with Fondazione Ugo Bordoni as Researcher in the Antennas and Propagation Laboratory. He joined the Department of Electronics, University "La Sapienza" in 1962 as an Assistant Professor, teaching applied electronics. In 1976, he was appointed Professor in the Chair of Antennas and Propagation and has been teaching this subject ever since. His current research interests are EM propagation in a turbulent atmosphere, microwave remote sensing of the atmosphere and earth's surface, and microwave radiometry of the atmosphere, particularly of cloud systems.